UCRL- 814 Rev

Copy 3.

UNIVERSITY OF CALIFORNIA — BERKELEY

UNCLASSIFIED

TWO-WEEK LOAN COPY

This is a Library Circulating Copy which may be borrowed for two weeks. For a personal retention copy, call Tech. Info. Division, Ext. 5545

RADIATION LABORATORY

DISCLAIMER

This document was prepared as an account of work sponsored by the United States Government. While this document is believed to contain correct information, neither the United States Government nor any agency thereof, nor the Regents of the University of California, nor any of their employees, makes any warranty, express or implied, or assumes any legal responsibility for the accuracy, completeness, or usefulness of any information, apparatus, product, or process disclosed, or represents that its use would not infringe privately owned rights. Reference herein to any specific commercial product, process, or service by its trade name, trademark, manufacturer, or otherwise, does not necessarily constitute or imply its endorsement, recommendation, or favoring by the United States Government or any agency thereof, or the Regents of the University of California. The views and opinions of authors expressed herein do not necessarily state or reflect those of the United States Government or any agency thereof or the Regents of the University of California.

UCRL-814 Rev.
Unclassified Distribution

UNIVERSITY OF CALIFORNIA

Radiation Laboratory

Contract No. W-7405-eng-48

UNCLASSIFIED

THE GAMMA RAY SPECTRUM RESULTING FROM CAPTURE OF NEGATIVE π MESONS IN HYDROGEN AND DEUTERIUM

Wolfgang K. H. Panofsky, R. Lee Aamodt and James Hadley

September 26, 1950

Berkeley, California

INSTALLATION	Number of Copies
Argonne National Laboratory	8
Armed Forces Special Weapons Project	1
Atomic Energy Commission - Washington	2
Battelle Memorial Institute	1
Brush Beryllium Company	1
Brookhaven National Laboratory	4
Bureau of Medicine and Surgery	1
Bureau of Ships	1
Carbide and Carbon Chemicals Division (K-25 Plant)	4
Carbide and Carbon Chemicals Division (Y-12 Plant)	4
Chicago Operations Office	1
Columbia University (J. R. Dunning)	1
Columbia University (G. Failla)	1
Dow Chemical Company	1
H. K. Ferguson Company	1
General Electric Company, Richland	3
Harshaw Chemical Corporation	1
Idaho Operations Office	1
Iowa State College	2
Kansas City Operations Branch	1
Kellex Corporation	2
Knolls Atomic Power Laboratory	4
Los Alamos Scientific Laboratory	3
Mallinckrodt Chemical Works	1
Massachusetts Institute of Technology (A. Gaudin)	1
Massachusetts Institute of Technology (A. R. Kaufmann)	1
Mound Laboratory	3
National Advisory Committee for Aeronautics	1
National Bureau of Standards	3
Naval Medical Research Institute	1
Naval Radiological Defense Laboratory	2
New Brunswick Laboratory	1
New York Operations Office	3
North American Aviation, Inc.	1
Oak Ridge National Laboratory	8
Patent Branch - Washington	1
Rand Corporation	1
Sandia Corporation	2
Santa Fe Operations Office	2
Sylvania Electric Products, Inc.	1
Technical Information Division (Oak Ridge)	15
Armament Division, Deputy for Research and Development (Capt. Glenn Davis)	1
Assistant for Atomic Energy, Deputy Chief of Staff (Col. Robert E. Greer)	1
Chief of Documents and Dissemination Branch (Col. J. E. Mallory)	1
USAF Assistant for Research Director of Research and Development, Deputy Chief of Staff (Col. B. G. Holzman)	1

INSTALLATION	Number of Copies
Electronic Systems Division (Mr. E. C. Trafton)	1
Chief of Scientific Advisors (Dr. Theodore von Karman)	1
USAF, Eglin Air Force Base (Major A. C. Field)	1
USAF, Kirtland Air Force Base (Col. Marcus F. Cooper)	1
USAF, Maxwell Air Force Base (Col. F. N. Moyers)	1
USAF, NEPA Office	2
USAF, Offutt Air Force Base (Col. H. R. Sullivan, Jr.)	1
USAF, Surgeon General, Medical Research Division (Col. A. P. Gagge)	1
USAF, Wright-Patterson Air Force Base (Rodney Nudenberg)	1
U. S. Army, Atomic Energy Branch (Lt. Col. A. W. Betts)	1
U. S. Army, Army Field Forces (Captain James Kerr)	1
U. S. Army, Commanding General, Chemical Corps Technical Command (Col. John A. MacLaughlin thru Mrs. Georgia S. Benjamin)	1
U. S. Army, Chief of Ordnance (Lt. Col. A. R. Del Campo)	1
U. S. Army, Commanding Officer, Watertown Arnsenal (Col. Carroll H. Deitrick)	1
U. S. Army, Director of Operations Research (Dr. Ellis Johnston)	1
U. S. Army, Office of Engineers (Allen O'Leary)	1
U. S. Army, Office of the Chief Signal Officer (Curtis T. Clayton thru Maj. George C. Hunt)	1
U. S. Army, Office of the Surgeon General (Col. W. S. Stone)	1
U. S. Geological Survey (T. B. Nolan)	2
U. S. Public Health Service	1
University of California at Los Angeles	1
University of California Radiation Laboratory	5
University of Rochester	2
University of Washington	1
Western Reserve University	2
Westinghouse Electric Company	4
R. F. Bacher (California Institute of Technology)	1
Cornell University	1
Total	140

Information Division
Radiation Laboratory
University of California
Berkeley, California

THE GAMMA RAY SPECTRUM RESULTING FROM CAPTURE OF NEGATIVE π MESONS IN HYDROGEN AND DEUTERIUM

Wolfgang K. H. Panofsky, R. Lee Aamodt and James Hadley

Radiation Laboratory, Department of Physics,
University of California, Berkeley, California

September 26, 1950

Abstract

π^- mesons produced in an internal wolfram target bombarded by 330 Mev protons in the 184-inch cyclotron are absorbed in a high pressure hydrogen target. The resulting gamma ray spectrum is analyzed outside the shielding of the cyclotron by means of a 30 channel electron-positron pair spectrometer. The principal results are: 1. The gamma rays result from two competing reactions: $\pi^- + p \rightarrow n + \gamma$ and $\pi^- + p \rightarrow n + \pi^0$; $\pi^0 \rightarrow 2\gamma$. 2. The ratio between the π^0 yield to the single gamma ray yield is $= .94 \pm .20$. 3. The mass difference between the π^- meson and the π^0 meson is given by 10.6 ± 2.0 electron masses. 4. The π^- mass is 275.2 ± 2.5 electron masses. The large mass difference between π^- and π^0 precludes the conclusion that the unexpectedly small π^0 to γ ratio is due to the small amount of momentum space available for π^0 emission. It rather indicates that π^0 emission is slowed down by the nature of the coupling of the π^0 field to the nucleons. The experiment has been repeated by substituting D_2 for H_2 in the vessel. The result is that the reaction $\pi^- + D \rightarrow 2n$ and $\pi^- + D \rightarrow 2n + \gamma$ compete in the ratio 2:1. The reaction $\pi^- + D \rightarrow 2n + \pi^0$ is absent.

THE GAMMA RAY SPECTRUM RESULTING FROM CAPTURE OF NEGATIVE π MESONS IN HYDROGEN AND DEUTERIUM

Wolfgang K. H. Panofsky, R. Lee Aamodt and James Hadley

Radiation Laboratory, Department of Physics,
University of California, Berkeley, California

September 26, 1950

I. Introduction

The classic experiments of Conversi et al[1] on the absorption of negative μ-mesons in matter gave the first definite information on the fact that the coupling of μ-mesons with nuclei is weak. On the other hand experiments on the absorption of π^- mesons[2,3] have confirmed the fact that π mesons are strongly coupled and that they have integral spin. This is evidenced by the fact that the process

$$\pi^- + p \rightarrow n^* \qquad (1)$$

taking place within a nucleus could not give rise to the large nuclear stars observed if an additional light particle of half integral spin had to be emitted, as in the absorption of μ^- mesons. Other than confirming this qualitative fact, the absorption of slow π^- mesons in matter has led to no quantitative information as to the nature of the coupling of π mesons to nuclei since the dominant time in the capture process is the slow-down time by ionization; once a π^- meson has arrived in the K shell of an atom, absorption is presumed to take place in $\sim 10^{-14}$ sec.

The case of π^- absorption in hydrogen is a singular one since clearly process (1) is forbidden by the conservation laws in the case of a free proton. Absorption of a π^- meson in hydrogen must thus lead to the emission of one or more additional particles. Excluding processes involving several spin 1/2 particles which are clearly too slow to compete, the possible processes which might result are:

$$\pi^- + p \rightarrow n + \gamma \qquad (2)$$

$$\pi^- + p \rightarrow n + 2\gamma \qquad (3)$$

$$\pi^- + p \rightarrow n + \pi^0 \qquad (4)$$

Prior to this work the possibility for process (4) rests of course on the possibility that the π^- might be sufficiently heavier than the π^0 to make the process energetically possible. Evidence from direct gamma ray production in a cyclotron target bombarded by 350 Mev protons[4] points to the existence of a π^0 of mass of the order of the π^- mass, but the center of the gamma ray spectrum cannot be localized with sufficient accuracy to decide the sign of the mass difference. Cosmic ray evidence[5-8] and particularly the observations of gamma-gamma coincidences observed from targets bombarded in the x-ray beam of the Berkeley synchrotron[9] have shown conclusively that a π^0 exists and that it disintegrates into two gamma rays and thus cannot have spin one. Recently Carlson, Cooper and King[10] have succeeded in analyzing positron-electron pairs observed in nuclear emulsions exposed at 70,000 feet in terms of neutral mesons. They show that the observed energy spectrum of such pairs is compatible with their origin from gamma rays from a π^0 meson of mass 295 $\pm$ 20 electron masses, where only the statistical error is included in the mass estimate. Carlson, Cooper and King also deduce the mean life τ of the π^0 meson to be $\tau < 5 \times 10^{-14}$ sec.

Preliminary reports of the present experiment[11] have qualitatively indicated that both processes (2) and (4) exist. However no accurate mass determination of the π^0 was possible and thus no very significant branching ratio between the processes could be inferred.

The evidence presented here excludes any appreciable competition from process (3). The reason is firstly a theoretical one: It appears to be difficult to construct a selection rule which would make double gamma emission compete effectively with single gamma emission. Secondly the double peaked energy distribution (see Fig. 10) of the emitted radiation practically excludes a two gamma process.

The details of the slow-down process of π^- in hydrogen have been discussed in considerable detail by Wightman[12]. The significant sequence of the process is:

1. Slow down of the fast meson by the ordinary stopping power mechanism ($\sim 10^{-10}$ sec). 2. Slow down by collisions with orbital electrons of velocities comparable with that of the meson ($\sim 10^{-12}$ sec). 3. Capture of the mesons in an outer orbit leading to an excited $\pi^- - H^+$ system[13]. 4. Reduction of energy of the neutral $\pi^- - H^+$ system to the lowest quantum state. This latter process principally is not radiative but is due to collisions of the neutral system with hydrogen molecules which leads by various mechanisms to the emission of an Auger electron, ($\sim 10^{-10} - 10^{-9}$ sec). In liquid or high pressure hydrogen the overall time to enter the K shell is thus sufficiently short to compete effectively with the π-μ decay time[14]. This is however true only if the H_2 density is sufficient. This point has been verified experimentally (see section VII). Capture in flight[15] corresponds to a life time of the order of 10^{-4} to 10^{-5} sec, depending on assumptions as to the interaction.

We can therefore conclude that at densities approximating that of liquid hydrogen all but of the order of 10^{-3} of the secondary radiations resulting from the capture of π^- in H_2 result either from absorption of the π^- meson from an inner shell or from π-μ decay; the π-μ decay branching is small.

II. Geometrical Arrangement. The hydrogen system.

The geometrical layout of the experiment is shown in Fig. 1. 330 Mev protons circulating in the internal beam of the 184-inch cyclotron strike a wolfram target 1/2 inch deep (parallel to the beam) and .040 inch thick (transverse to the beam). Wolfram was chosen since the π^- cross section measurements of Weissbluth[16] showed that a heavy element favors π^- production. Also auxiliary measurements on beam penetration and "scattering out" showed that a high density target was desirable here from the point of view of total meson yield. Finally, as discussed later, the background in this experiment is principally produced by high energy protons elastically scattered and striking the hydrogen vessel. At this energy scattering at the angles in question

is principally diffraction scattering; heavy elements produce a smaller diffraction angle.

The π^- mesons enter the high pressure hydrogen through the walls of the pressure vessel shown in Fig. 2. In order to produce maximum yield, the wall thickness is limited in order that the mesons absorbed in the hydrogen are those produced at a sufficiently low energy to correspond to a rising portion of the meson yield curve as a function of meson energy. Such considerations limit the wall thickness to ~ 8 gm/cm^2. On the other hand a density close to that of liquid H_2 is desirable by the capture considerations given above. The use of liquid H_2 was not advisable here owing to the difficulty of cooling a long horizontal filling tube required by the geometry of the cyclotron. The vessel shown in Fig. 2 operates at a factor of safety of about 2.5 when maintained at 2700 p.s.i. and at liquid N_2 temperature. The specific gravity[17] under these conditions is .046. The factor of safety mentioned above makes use of the appreciable increase in strength of stainless steel at low temperature[18]. The outer jacket is fed by an external liquid N_2 Dewar vessel. The pressure vessel is filled by an external oil piston pressure pump* fed by commercial H_2, dried and purified in a liquid N_2 trap. A flow diagram of the arrangement is shown in Fig. 3. A similar system is used for deuterium with certain modifications to permit recovery.

III. The Pair Spectrometer.

Since the expected pair spectra from processes (2) and (4) exhibit discontinuities, satisfactory analysis and also good signal to background ratio requires a spectrometer with a large number of channels. Since the counting rates in this experiment are limited entirely by absolute available intensity and not by errors introduced by accidental coincidences, etc., Geiger counters as used by Lawson[19] seem to offer the

*Manufactured by: American Instrument Company, Superpressure Division, Silver Spring, Maryland.

best solution to the multiple channel problem. The geometrical layout of the pair sepctrometer is shown in Fig. 4. The magnet has a useful gap of 3.5 inches and a maximum field of 14,000 gauss although for this experiment only fields of the order of 5000 - 10,000 gauss were used. The pole piece is in the shape of a 90° triangle, the hypotenuse of the triangle being 30 inches. The pole is widened near the converter position in order to improve the uniformity of the field near the converter; field uniformity is not as essential near the counters as it is near the converter. There is no specific advantage to the choice of 90° for the triangle apex angle; the angle was defined principally by arguments of size and weight. A 90° apex angle (and hence a 90° deflection angle!) provides for first order horizontal focusing for particles of the same energy originating in different parts of the converter; this is however not an essential consideration if one is interested only in the sum of the energy of the two pair fragments.

The resolving power of a pair spectrometer of this type is essentially defined by three factors: 1. Channel width. 2. Multiple scattering in the converter. 3. Radiation straggling of the pair members. A feature of the triangular design is the fact that the energy width due to multiple scattering is constant. The converter thickness has been chosen such that the combination of the latter two widths approximately matches the first. This condition can only be approximately achieved since the ratio of the radiation error to the scattering error varies as the pair energy. The choice of converter material is not critical since pair conversion efficiency, multiple scattering and radiation straggling only depend on the number of radiation lengths of converter used. Tantalum converters were used in this experiment. The choice of triangular shape of magnet and the analysis of the resolution of such a magnet are due to Professor Edwin McMillan. The initial design of the pair spectrometer magnet was carried out by Herbert F. York and the mechanical engineering design is due to

Robert Meuser; the authors are greatly indebted to them for their contributions.

Due to the high singles rates (approximately 3 counts/sec) of the Geiger counters (Victoreen type 1B85) and the low true pair rate (approximately 30 c/hour), additional selection of events is necessary. This is provided by 4 large proportional counters (see Fig. 4) backing up the counter arrangements. A pair event is selected by a quadruple coincidence count in the proportional counters; this quadruple coincidence opens a gate which passes the amplified Geiger pulses into a recorder. This recorder consists of 30 pens marking voltage sensitive paper on a rotating drum. A typical event thus appears as two dots in the appropriate channels. The arrangement of the electronic components is shown in Fig. 5. The counting rate is sufficiently slow to permit this mechanical means of recording. The proportional counter gate width is 1.5 μ-sec; accidental counts are entirely negligible; the counting rate loss due to Geiger counter dead time is estimated at less than 2 percent.

The magnet is fed by a motor generator set electronically regulated; the magnetic field has been calibrated against the magnetic moment of the proton; during runs the fields are monitored by current readings with a shunt and potentiometer or with a proton moment apparatus if the accuracy is needed.

The sensitivity of a pair spectrometer is not constant over the energy range covered by the instrument. This is due to a) the variability of number of channels available to record the pair fragments of a given total energy. b) The variation of pair production cross section with energy. c) The variability of loss by scattering. It can be shown easily that c) can be neglected in this geometry. The correction curve of the instrument due to cause a) and b) is given in Fig. 6.

IV. Operation of Runs.

Before every run the spectrometer is checked by using gamma rays directly produced in the cyclotron target[4]. The yield of the direct gamma rays is sufficient to permit the plateaus of all counters to be checked with good statistics. Also all Geiger channels are checked for singles rates by removing the gate formed by the proportional counters. The target and pressure vessel are then moved so that the primary target is well shielded from the spectrometer and the hydrogen vessel is aligned with the collimators and the spectrometer. (See Fig. 1.)

Readings are made with the pressure vessel either evacuated or pressurized with H_2 or D_2. If the vacuum runs are to represent the true background it is necessary that no other process (e.g., scattering of protons from the target) produces γ rays in hydrogen. This assumption receives support from experiments by Crandall, Hildebrand, Moyer and York[20], indicating that the production cross section for gamma ray production by bombardment with 345 Mev protons in hydrogen is less than 2 percent of the cross section in carbon. This means that if a sufficient number of primary protons were scattered into the hydrogen to produce gamma rays of significant intensity, then the background due to gamma rays hitting the steel vessel would be much higher. It therefore appears certain that the gamma rays depending on the introduction of the H_2 are not produced by fast particle collisions in H_2. This argument is not as significant in the case of D_2. As a further link in the qualitative interpretation of the experiment it was shown that no statistically significant gamma ray counts beyond background were produced by the introduction of He into the pressure vessel. This check was done with relatively poor statistics; a positive helium effect in the form of a broad gamma ray spectrum of 10 percent total intensity of that observed in H_2 is not excluded by the data.

The background has the general character of the gamma ray spectra observed by Bjorklund, Crandall, Moyer and York[4] at 180° from the target. The background is almost certainly due to protons scattered by the primary target onto the steel jacket of the pressure vessel and other parts of the cyclotron. The background is negligible in the 130 Mev region but is of the same order of intensity as the H capture gamma rays in the 70 Mev region.

V. Gamma Ray Spectra from Hydrogen.

As can be seen from the spectrometer response curve (Fig. 6) it is not possible to cover the entire spectrum of the spectrometer with good efficiency. Accordingly different runs were made with the spectrometer set with its central point at a) single gamma ray peak, b) center between the two peaks to permit easy relative area measurement, and c) π^0 peak.

a. The high energy peak. The π^- mass.

Figure 7 shows the spectrum observed with the spectrometer maximum set near the high energy peak. Note that the "π^0 peak" also appear clearly.

Since the position of the single gamma peak gives a precise measurement of the π^- mass it is a matter of considerable interest to analyze the observed peak accurately in terms of resolving power of the pair spectrometer. Fig. 8 shows plotted individually the resolving power curves due to the three principal causes of finite resolving power. The first cause is the finite channel width. This gives rise to a triangular resolution R_1 (E) of base equal to twice the channel width, which is 5.36 Mev. The second cause is the multiple Coulomb scattering in the converter. One can show easily that if $\langle\theta\rangle$ is the root mean square plane projected scattering angle[24] of an electron of energy of one half the gamma energy after having passed through the full converter thickness, then the fractional R.M.S. error in gamma energy is

given by

$$\delta = \frac{\delta E_\gamma}{E} = (\sqrt{2}\langle\theta\rangle)/3 \qquad (5)$$

This gives a resolving power R_2 (E) given by

$$R_2(E) = e^{-\frac{(E - E_\gamma)^2}{2\delta E_\gamma^2}} \qquad (6)$$

plotted in Fig. 8b.

The third cause is radiation straggling of the outgoing pair represented by a resolving power curve R_3 (E). Let, in the notation used by Heitler[21] w(y)dy be the probability that the energy of a single electron has decreased to e^{-y} times its initial value after traversing a thickness t. Let W(p)dp be the resultant probability that an outgoing pair fragment has retained a fraction between p and p + dp of its energy of formation. W(p) can be generated by averaging w(y) over the converter thickness. Let $P(E_1,E)dE_1$ be the probability that a pair fragment have an energy between E_1 and $E_1 + dE_1$ for a total pair energy E. It can be shown that the probability $\pi(f)df$ that the resultant pair shall have retained a fraction between f and f + df of its initial energy is given by:

$$\pi(f)df = df\int_{E_A}^{E_B} dE_1 \left\{ \int_{1 - \frac{E_\gamma}{E_1}(1-f)}^{1} \left(\frac{E_\gamma}{E_\gamma - E_1}\right) W(p) W\left(\frac{E_\gamma f - pE_1}{E_\gamma - E_1}\right) P(E_1, E_\gamma) dp \right. \qquad (7)$$

Here E_A and E_B are the pair fragment energy limits defined by the spectrometer. This integral has been evaluated using the forms $P(E_1, E_\gamma)dE_1 = dE_1/E_\gamma$ and $W(p) = K/(1 - p)^{1-\alpha}$ where α was fitted to the computed radiation curves. The result

shows that the resolving power has the approximate form:

$$R_3(E) = \frac{1}{(E_\gamma - E)^{1-2a}} \qquad E < E_\gamma$$
$$= 0 \qquad E > E_\gamma \tag{8}$$

This is plotted in Fig. 8c for $a = .92$, $E_\gamma = 132$ Mev. This corresponds to a .020 inch tantalum radiator. The three resolving powers are then combined numerically by a successive folding* process; the resultant curve is shown in Fig. 8d.

Fig. 9 shows both the final resolving power curve and the experimental data superimposed to give optimum fit. A logarithmic scale is chosen for the intensity to permit satisfactory normalization. It is observed that the fit is quite satisfactory.

It is estimated that the probable error in fitting the curves is ± .8 percent. The remaining errors deal with the establishment of the energy scale.

The magnetic field was monitored continuously during operation by means of a magnetic moment of the proton apparatus. The probable error in magnetic field measurement of a chosen reference point is estimated at ± .03 percent. The magnetic field was mapped with a flip coil accurate in relative measure to an accuracy of .1 percent probable error. Trajectories were laid out to determine the small corrections for field non-uniformity. It is estimated that the error due to uncertainty in trajectory layout is ± .3 percent probable error. The geometry was laid out accurately to ± .1 percent probable error. As a result the overall probable error is ± .9 percent, the principal contribution being the accuracy of curve fitting. We thus obtain

$$M_{\pi^-} = 275.2 \pm 2.5 \text{ electron masses}$$

A more accurate measurement based on this method is planned.

---

* The "fold" f(x) of two functions g(x) and h(x) is defined by $f(x) = \int_{-\infty}^{+\infty} g(t-x)h(t)dt$

The excellent agreement of this result with the photographic work[22,23] confirms also the argument that we are in fact observing process (2).

b. The low energy peak.

The spectrum in the neighborhood of the low energy peak is shown in Fig. 10. The resolving power at this energy is principally defined by multiple scattering of the pair fragments. The resolving power is again calculated as above and has been plotted in Fig. 10. Note that the resolution is sufficient to assure that the width of the curve of Fig. 10 is real rather than instrumental. Experimentally we take the lower and upper limits at $W_1 = 53.6 \pm 2.8$ Mev and $W_2 = 85 \pm 2.8$ Mev, respectively. The probable errors are estimated on the basis of the uncertainty in fit of these computed curves to the experimental data.

Analysis of the process

$$\pi^- + p \rightarrow n + \underset{\hookrightarrow 2\gamma}{\pi^0} \qquad (9)$$

is based on the following physical picture: Since essentially all the observed radiation results from π^- mesons of initial velocity $\beta \sim 1/137$, we can assume that the kinetic energies of the π^0 plus that of the neutron in process (9) are essentially equal to the mass differences involved. Since the Doppler width of the emitted gamma ray is proportional to the momentum of the π^0, the following equation can be deduced:

$$\delta = \Delta + (M_{\pi^-} - \Delta)\left\{1 - \left[1 - \frac{2(\pi^- + M_p)M_n \quad a}{(M_n - \Delta)^2}\right]^{1/2}\right\} \qquad (10)$$

where

$$a = \frac{1}{M_n}\left\{\sqrt{M_n^2 + \Delta W^2} \quad - M_n\right\} \approx \frac{\Delta W^2}{2M_n^2}$$

Here δ is the mass difference between π^- and π^0, Δ is the neutron-proton mass difference[25] and ΔW is the width of the peak: $\delta - \Delta$ depends thus essentially on the

width of the peak of Fig. 10.

It can easily be shown statistically that the expected distribution of γ energies is uniform on an energy scale between the two Doppler limits. The sum of the lower and upper limits of the γ peak represents the total relativistic energy of the π^0; it is thus equal to the π^- mass less the neutron-proton mass difference and the neutron recoil energy; thus if S is the sum of the upper and lower spectral limits

$$S = M_{\pi^-} - \Delta - \frac{1}{2}\frac{(\Delta W)^2}{M_n} \qquad (11)$$

Fig. 11 shows graphically the relation between the energy limits and the masses involved. The ordinates and abscissae of Fig. 9 are W_2 and W_1, the upper and lower limits respectively, and the measured values are indicated. Lines of Constant $\pi^- - \pi^0$ mass difference (δ) are practically of the form $W_2 - W_1$ = const., while lines of constant π^- mass are of the form $W_2 + W_1$ = const. Both these functions have been plotted, in addition to the lines of constant π^0 mass. The measured values of W_1 and W_2 and their probable errors generate an ellipse of error in the $W_2 - W_1$ plane which is given here. Accordingly

$$\delta = M_{\pi^-} - M_{\pi^0} = 5.4^{+1.1}_{-.9} \text{ Mev.} \quad 5.4 \pm 1.0 \text{ Mev} = 10.6 \pm 2.0 \text{ electron masses} \qquad (12)$$

From the diagram:

$$M_{\pi^0} = 135 \pm 4 \text{ Mev} = 265 \pm 8 \text{ electron masses}$$

Using the mass values determined above for the π^- mass, Eq. (12) leads to the π^0 mass:

$$M_{\pi^0} = 264.6 \pm 3.2 \text{ e.m.}$$

Further reduction of the probable errors of the π^- mass is, however, anticipated[23].

c. Branching ratio between π^0 and γ emission.

A run was made with the peak of the pair spectrometer intensity curve located at 100 Mev. This gives somewhat poorer statistics on either the low energy or the

high energy peaks but permits a measurement of the branching ratio. The resulting curve is shown in Fig. 12. Fig. 12 also shows a rectangular profile of area equal to the total intensity of the low energy group and of width equal to the width of the low energy peak in Fig. 10. Considering the fact that two photons are emitted per π^0 disintegration we obtain a braching ratio of

$$\frac{\Gamma_{\pi^0}}{\Gamma_\gamma} = .94 \pm .20 \qquad (13)$$

The probable error quoted is due to the statistics of the data and a reasonable allowance for the uncertainty in the spectrometer sensitivity curve. In interpreting this branching ratio it should be noted that, from Fig. 10

$$\frac{p}{M_{\pi^0} c} = .23 \pm .03 \qquad (14)$$

gives the momentum of the π^0 in process (4).

d. Energy distribution of pair fragments.

The pair fragment energy of the pairs entering into the gamma ray spectrum of Fig. 10 has been tabulated as a check on the performance of the pair spectrometer. Although the statistics are insufficient to provide data of interest to pair theory, it is relevant to show that the probability of division of a pair is essentially constant as a function of the division percentage[21]. Fig. 13 shows a graphical representation of the number of pairs of fragment energy E_1 and E_2 plotted as a function of the division fraction $E_1/(E_1 + E_2)$. The instrument does not permit recording of all possible division ratios, since (see Fig. 4) the counter arrangement does not reach to the converter and is limited in radial extent. Accordingly the scale of intensities of Fig. 13 is weighted inversely to the gamma ray energy interval which contributes to the particular division ratio. Division ratios are given only in the range $.2 < E_1/(E_1 + E_2) < .8$. It is seen that within statistics the distribution is uniform as theoretically predicted.

VI. Runs with materials other than hydrogen or deuterium.

In the beginning stages of these experiments hydrogenous compounds were used in place of the high pressure H_2 vessel[26]. The pair spectrometer used had only a single channel 30 percent wide but the instrumentation was sufficient to show the presence or absence of gamma ray yield within certain limits.

Let f = fraction of π^- absorbed which is finally absorbed on a hydrogen nucleus. The expected and observed intensities are tabulated below (Table I).

Table I

Tabulation of γ ray yield from the absorption of π^- mesons in hydrogenous materials. f = fraction of π^- mesons absorbed ultimately on a proton.

Absorbing Material	γ-ray energy	Expected Count c/hr	Observed Count c/hr
CH_2	135 Mev	5000 f	0 ± 2
LiH	135 Mev	1500 f	.5 ± 2
LiH	68 Mev	1500 f	-1 ± 4

The "expected count" was computed from evaluation of the geometry and the conversion yields. The calculations were checked by observing the γ rays originating directly from the target[4]. The expected count is estimated to be certainly correct to within a factor of 3. We can conclude therefore that $f < 2 \times 10^{-3}$ for CH_2 and $f < 6 \times 10^{-3}$ for LiH. It is thus clear that the absorption probability is not simply proportional[14] to Z, but that a special mechanism favors the absorption on a higher Z nucleus. This mechanism operates as follows: Once a π^- meson is captured on a hydrogen nucleus in an outer Bohr orbit, the atom loses its electron and hence its chemical binding. The life-time

of the resulting excited π^- - H system toward radiation into the K shell is long compared to the collision time with other nuclei; during the collision of the π^- - H system with a heavier nucleus, the probability is large that the π^- be captured by the heavier nucleus with the consequent production of a nuclear star, rather than a γ ray. Approximate estimates of the value of f have been made on the basis of this mechanism and are not inconsistent with the observations.

It has been suggested by Barkas[27] that π^0 emission might compete with nuclear stars induced by π^- capture. This is energetically possible if the mass of the capturing nucleus (Z,A) is less than that of the resulting nucleus (Z-1,A) by less than the π^- - π^0 mass difference, δ. In particular if the corresponding β transition (Z-1) $\rightarrow$ Z is allowed, the γ rays from the disintegration of the resulting π^0 might be observable. This possibility is now being studied. A special case in this class is absorption in deuterium, studied theoretically by Marshak and his coworkers[28]; we shall discuss the process in the next section.

VII. Absorption in deuterium.

a) Discussion of the process.

The absorption of π^- mesons in deuterium can lead to processes analogous to those outlined above, in addition to pure heavy particle emission in the form of two neutrons. We consider thus the processes

$$\pi^- + D \rightarrow 2n \tag{15}$$

$$\pi^- + D \rightarrow 2n + \gamma \tag{16}$$

$$\pi^- + D \rightarrow 2n + \pi^0 \tag{17}$$

Process (15) will lead to monoenergetic neutrons. At first sight one might expect that process (16) would lead to a very broad γ ray spectrum. This is actually not so, since if the γ ray has low energy the conservation laws are satisfied only if the neutrons are emitted nearly exactly in opposite directions. Consequently large

γ ray energies will be favored. One can show easily that, in the absence of angular correlation between the particles, the γ ray distribution is given by

$$N_\gamma dE = \sqrt{W_o - E} \cdot E^2 \, dE \qquad (18)$$

where $W_o = M_n - M_D - 2M_n = 1/4 \frac{W_o^2}{M_n c^2}$ is the energetic upper limit. (See Fig. 14.) Actually we shall see that the spectrum is still considerably narrower.

The spectrum of process (17) is expected again to lie between boundaries defined by the Doppler shift of the moving π^o. Due to the extra energy required in dissociating the deuteron, the peak is expected to be narrower. Using the above value for the π^o mass, the kinetic energy of the π^o is approximately 1.9 ± 1.0 Mev. Process (17) is thus energetically permitted nominally although the π^o mass accuracy is not sufficient to establish this fact beyond reasonable doubt.

b) Experimental results.

Two experimental runs on deuterium were performed in the identical geometry, pressure, temperature and spectrometer setting to the conditions under which the high energy spectrum of the absorption of π^- in H_2 was taken (Fig. 7). Accordingly we feel safe in comparing the yields of the two processes by assuming that the same number of π^- mesons reach the K shell in the two cases for a given proton bombardment of the primary target. There might be two qualifications to this statement: both with H_2 and D_2 we are dealing with the same number of electrons/cm^3 and thus comparable stopping power. The time required to reach an outer Bohr orbit is thus identical in the two cases. However the time required for transition to lower states depends on collision processes[12]; the situation here is thus not quite identical in the two cases. Furthermore possible capture from an orbit other than an S orbit depends of course on the end product in the process in question.

An experiment was carried out to determine whether an appreciable number of π^-

mesons were lost by π-μ decay before reaching the K shell. If the life time of the energy reduction process by collison were comparable to the π-μ decay time (contrary to the calculation by Wightman[12]), then the yield of γ ray from H_2 would fall off more rapidly with reduced density than the density itself. The following table (Table II) shows the observed γ ray intensities at the usual operating pressure (2700 psi) and at reduced pressure.

Table II

Tabulation of the relative γ-ray yields from H_2 at 2700 psi and 1300 psi. Intensities are tabulated in terms of counts/minute. Total quadruple coincidences in the proportional counters total number of recorded pairs, and the pairs corresponding to the high energy peak only are tabulated.

	Intensity in counts/minute		
	2700 psi	1300 psi	Ratio
Total number of quadruple coincidences	.853 ± .033	.523 ± .042	1.63 ± .14
Total number of γ rays recorded on multiple channel unit	.302 ± .021	.190 ± .027	1.60 ± .25
γ rays recorded in the high energy peak only	.213 ± .013	.121 ± .017	1.74 ± .27
Density	.046	.028	1.65

Clearly no significant non-linear decrease is observed. Accordingly we conclude that in agreement with Wightman[12], no significant π-μ loss occurs and hence the intensity comparison between H_2 and D_2 γ yields are valid. The evidence for process (15) thus rests on a good quantitative basis. A separate experiment in progress[29] also tentatively confirms the existence of fast neutrons correlated to the presence of deuterium

in the pressure vessel.

The spectrum corresponding to the spectrum of Fig. 7 is shown in Fig. 15. The first conclusion is that its spectrum does not conform to the momentum space function plotted in Fig. 14. The reason is that the two slow neutrons involved cannot be considered free but will interact to favor a small relative velocity between the neutrons. This will result in a spectrum peaked toward high energy. The effect is analogous to the high energy peak observed in the π^+ peak formed in p-p collisions[28]; there the n-p interaction favors a high π^+ energy. The low binding energy of the deuteron will also favor low relative velocities between the two neutrons.

The second result is the apparent absence of the π^0 peak. A separate run was made with the spectrometer centered at 70 Mev in order to place more rigid limits on the π^0 intensity. The observed counts are tabulated below. Since the H_2 spectrum shown in Fig. 7 was obtained under comparable conditions we can directly compare the γ ray yields. This comparison is given in the table below (Table III).

Table III

Summary of relative intensities of various processes obtained as a result of π^- capture in various materials. Tabulated values are given in counts per minute. In the case of single γ-ray processes this represents the counting rate of the spectrometer; in the case of π^0 emission it represents 2 times the spectrometer rate. The "two fast neutrons" count does not represent direct observation but only the intensity inferred by balancing counts between hydrogen and deuterium absorption.

Particle Emitted \ Absorber	H	D
π^0	.45 ± .09 c/m	-.007 ± .020 c/m
Single γ	.470 ± .046 c/m	.275 ± .034 c/m
two fast neutrons		.65 ± .11

The intensity of the fast neutron yield (process 15) is only inferred from the intensity balance with hydrogen and does not represent direct observation.

VIII. Conclusions.

In a qualitative sense the results reported here confirm some of the already reasonably well established facts concerning π mesons: 1. The existence of the monochromatic high energy peak from hydrogen proves that the π^- meson is a boson. 2. A π^0 meson exists[5,10] and it disintegrates into two photons; it thus must be a spin 0 particle. 3. The electrostatic self energy or other causes make the π^- heavier than the π^0 by about 11 electron masses. 4. As long as emission of the π^0 could be in an S state only, the π^0 and π^- must be particles of identical parity properties. Considering the large kinetic energy of the π^0 emitted in process (4), this conclusion is no longer rigorous.

A quantitative result which might permit interpretation at the present time is the branching ratio between π^0 and γ emission and the ratio between 2n and γ emission in deuteron capture. By elementary notions mesons are strongly coupled to nuclei while photons are weakly coupled; therefore a branching ratio close to unity seems paradoxical, since the π^0 phase space factor $\frac{p}{M_{\pi^0}c}$ is as large as 1/4. Processes (2) and (4) are essentially the inverse of photo meson production and of "charge exchange" scattering of π mesons on nucleons. By a detailed balancing argument the ratio of cross section for such processes would be of the order of unity. Actually, at high energies, it appears as if the photo production cross sections for mesons are well below nuclear interaction cross sections of mesons. This argument is of course weakened by the fact that the energies involved in the capture experiment and the inverse processes mentioned are dissimilar.

A very analogous difficulty appears in the case of the deuterium results. Process (15) is essentially the inverse of meson production in like particle collisions[28] and process (16) is essentially the inverse of the photoproduction of π^- mesons[30]; experimentally the latter process has a very much smaller cross section than the

production cross section in like particle collisions. Again a dependence of the matrix elements on π^- energy could remove the contradiction.

A definite result which can be deduced from the inferred presence of the fast neutron yield is the fact that the π^- is not a scalar particle. This is clear since the process

$$\underset{\text{S-orbit}}{\pi^-} + \underset{{}^3S}{D} \longrightarrow \underset{{}^1S \text{ or } {}^3P}{2n} \tag{19}$$

violates either parity or angular momentum conservation for a scalar π^-. Capture from a p-state might weaken this selection rule; however calculations by Brueckner and Watson[31] indicate that the lifetime for radiation from a p orbit is very short compared to the capture time so that this effect can be neglected.

The absence of the π^0 peak in the case of π^- capture by deuterium is not surprising. If the π^- and π^0 are particles of equal parity, then in the process

$$\underset{\text{S-orbit}}{\pi^-} + \underset{{}^3S}{D} \longrightarrow \underset{{}^3P}{2n} + \underset{\text{P-wave}}{\pi^0} \tag{20}$$

both the π^0 and the two neutrons must be emitted in odd states of angular momentum as indicated, in order to obey conservations of parity and angular momentum and the exclusion principle. This effect[32] produces a greatly retarded yield at the small π^0 energy available.

Direct calculations of the branching ratio based on various combinations of vector character and coupling have been made by several authors[31,32]. The formal perturbation calculations show that the number of possibilities of meson character and coupling is greatly reduced by the results of this experiment. In fact only a pseudoscalar meson for both π^0 and π^- meson gives reasonable numerical results.

It has been shown quantitatively by Brueckner, Serber and Watson[31] that the variability of the matrix element predicted by the comparison of branching ratio measurements reported here with the inverse processes is subject to experimental check by

measurements of the excitation function of meson production in p-p collisions.

As a further remark it might be mentioned that there exists here of course no positive proof that the π^0 mesons observed here is identical with the π^0 observed as produced by nuclear collisions[4-8,10] and photo production[19], but the inference appears justified.

IX. Acknowledgements.

The authors have benefited greatly by the active cooperation of many members of this Laboratory. In particular the help of Dr. Herbert F. York during the first phases of the experiment has been indispensable. We are also indebted to Robert Meuser and Hugh Smith for mechanical design, to Mr. Alex Stripeika for assistance in electronics and to the cyclotron crew under Mr. James Vale for the bombardments and assistance in the adjustments. The authors have also gained valuable information by discussions with Drs. Marshak, Serber, Wick, Brueckner and Watson. Mr. Robert Phillips has actively participated in the execution of the experiment and has been of invaluable assistance.

References

1. Conversei, Pancioni and Piccioni, Phys. Rev. 68, 232 (1945).

2. See e.g., Manon, Muirhead and Rachat, Phil. Mag. 41, 583 (1950).

3. F. Adelman and S. Jones, Science 111, 226 (1950).
W. Cheston and L. Goldfarb, Phys. Rev. 78, 320A (1950).

4. Bjorklund, Crandall, Moyer and York, Phys. Rev. 77, 213 (1950).

5. W. Fretter, Phys. Rev. 73, 41 (1948); Phys. Rev. 76, 213 (1949).

6. C. Y. Chao, Phys. Rev. 75, 581 (1949).

7. Gregory, Rossi and Tinlot, Phys. Rev. 77, 299 (1949).

8. Kaplon, Peters and Bradt, Phys. Rev. 76, 1735 (1949).

9. Steinberger, Panofsky and Steller, Phys. Rev. 78, 802 (1950).

10. Carlson, Cooper and King, Phil. Mag. 41, 701 (1950).

11. W.K.H. Panofsky, Post Deadline Paper, New York Meeting A.P.S., 1950.
Panofsky, Aamodt and York, Phys. Rev. 78, 825 (1950).

12. A. S. Wightman, Thesis, Princeton University (June, 1949) and Phys. Rev. 77, 521 (1950).

13. E. Fermi and E. Teller, Phys. Rev. 72, 399 (1947).

14. J. R. Richardson, Phys. Rev. 74, 1720 (1948).
E. A. Martinelli and W. K. H. Panofsky, Phys. Rev. 77, 465 (1950).
Chamberlain, Mozley, Steinberger and Wiegand, Phys. Rev. 79, 394 (1950).
M. Jakobsen, private communication.

15. R. Marshak and A. S. Wightman, Phys. Rev. 76, 114 (1949).

16. M. Weissbluth, Phys. Rev. 78, 86A (1950).

17. Johnston, Berman, Rubin, Rifkin, Swanson and Corak, MDDC-850.

18. E. E. Thum, "The Book of Stainless Steels", 2nd Edition, p. 376, American Society for Metals, Cleveland, 1935.

19. J. L. Lawson, Phys. Rev. 75. 433 (1949).

20. Crandall, Hildebrand, Moyer and York, private communication.

21. See e.g., Heitler, Theory of Radiation, Oxford, 1944, p. 223 ff.

References (cont.)

22. Gardner, Barkas, Smith and Bradner, Science 111, 191 (1950).

23. Frances Smith, private communication.

24. B. Rossi and K. Greisen, Rev. Mod. Phys. 13, 240 (1941).

25. R. E. Bell and L. G. Elliott, Phys. Rev. 74, 1552 (1948).

26. W.K.H. Panofsky and H. York, Phys. Rev. 78, 89A (1950).

27. Walter H. Barkas, private communication.

28. Cartwright, Richman, Whitehead and Wilcox, Phys. Rev. 78, 823 (1950).
Vincent Z. Peterson, Phys. Rev. 79, 407 (1950).

29. K. Crowe and H. F. York, private communication.

30. Peterson, McMillan and White, Science 110, 579 (1949).

31. Brueckner, Serber and Watson, private communication.

32. Stephen Tamor, Phys. Rev. 79, 221 (1950).
R. E. Marshak, private communication.

Figure Captions

Fig. 1. Geometrical arrangement of π^- capture experiment. π^- mesons produced in a primary wolfram target of the 184-inch cyclotron are captured in the H_2 pressure vessel. The resultant gamma rays are collimated and leave the cyclotron shielding through a hole tapering from 2 inches to 3 inches in diameter. The gamma rays are then analyzed by a pair spectrometer.

Fig. 2. High pressure vessel used for absorption of H_2 and D_2. The vessel is constructed of stainless steel machined as indicated. The load is carried by threads with the weld serving as a seal only. The outer stainless steel liquid N_2 jacket (.010" thick) is soft soldered to the thick portion of the main vessel.

Fig. 3. Flow diagram of H_2 pressure system. H_2, purified in a liquid N_2 trap, is admitted into the pressure chamber above pump and at tank pressure. The pressure is then raised by displacing the H_2 in the pressure chamber with oil pumped as shown.

Fig. 4. Outline diagram of pair spectrometer. The converter, Geiger counter array and the proportional counters are shown. Note the geometry of the pole piece to give a uniform field in the area of the converter.

Fig. 5. Block diagram of electronic components.

Fig. 6. Multiplication factor to be used to reduce observed counting rates to gamma ray intensity. This factor arises from: a, variation of pair production cross section with energy, and b, number of available channels into which a given total pair energy can divide.

Fig. 7. Pair spectrum of gamma rays produced by capture of π^- in H_2. Center of spectrometer set near 130 Mev.

Fig. 8. Curves showing the components of the resolving power curve of the spectrometer.

a) Resolving power due to finite channel width.

b) Resolving power due to multiple scattering of pairs in converter.

c) Resolving power due to radiation straggling of outgoing pair.

d) "Fold" of a, b, and c giving total resolving power.

Fig. 9. Pair spectra of gamma rays from the process $\pi^- + H \rightarrow n + \gamma$ plotted on a logarithmic scale. Plotted (solid line) also is the theoretical resolving power curve adjusted for best fit. The origin of the resolving power curve marks the energy value of the gamma ray on the abscissa of the pair spectrum.

Fig. 10. Pair spectrum of gamma rays presumably due to the process $\pi^- + H \rightarrow n + \pi^0 \rightarrow n + 2\gamma$. Plotted also is the theoretical spectral shape assuming that the spectrum lies between the limits of 53.6 Mev and 85 Mev. The estimated probable errors of these limits are indicated.

Fig. 11. Graphical representation of the relations defining the meson masses in terms of the lower and upper limit of the spectrum of Fig. 10. The ordinate and abscissa are the upper and lower limits respectively. Plotted on this graph are: a) The experimental values and the probable errors of the lower and upper limits. b) The ellipse (a circle in this case) in the coordinate plane representing the area of 50 percent probability for the quoted masses. c) The lines of constant π^- mass. d) The lines of constant $\pi^- - \pi^0$ mass difference. e) The curves of constant π^0 mass.

Fig. 12. Pair spectrum resulting from the absorption of π^- mesons in hydrogen. The center of the spectrometer is set near 100 Mev. The spectrum clearly shows the separation between the processes (2) and (4). The branching ratio between these reactions can be derived from this spectrum.

Fig. 13. Energy distribution of pair fragments. The frequency of occurrence of a given energy division is plotted against the energy fraction $E_1/(E_1 + E_2)$; the measurements cover the range $.2 < E_1/(E_1 + E_2) < .8$. The ordinate does not represent the actual count but is divided by the gamma ray energy interval contributing to the particular division ratio interval. It is seen that the distribution is uniform within statistics.

Fig. 14. Plot of the function giving the energy distribution of gamma rays from the process $\pi^- + D \rightarrow 2n + \gamma$ for a constant matrix element.

Fig. 15. Pair spectrum resulting from π^- capture in deuterium. The spectrometer center is set near 130 Mev.

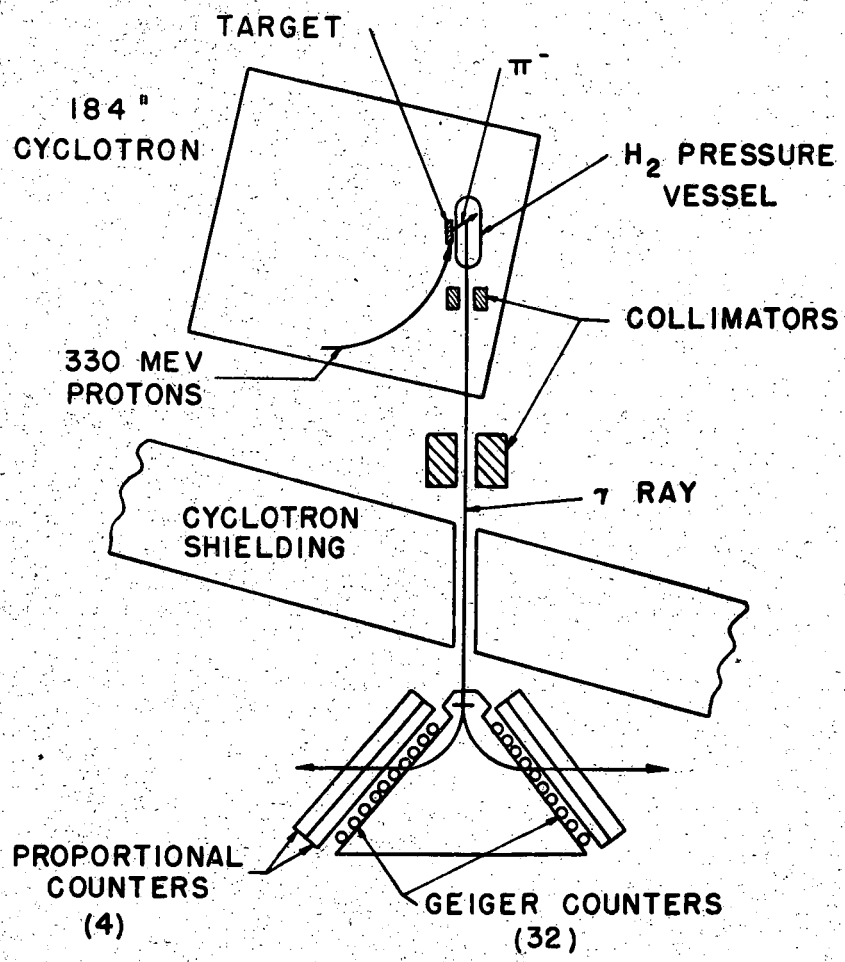
TARGET
π⁻
184"
CYCLOTRON
H2 PRESSURE
VESSEL
COLLIMATORS
330 MEV
PROTONS
γ RAY
CYCLOTRON
SHIELDING
PROPORTIONAL
COUNTERS
(4)
GEIGER COUNTERS
(32)

FIG. 1

MU 791

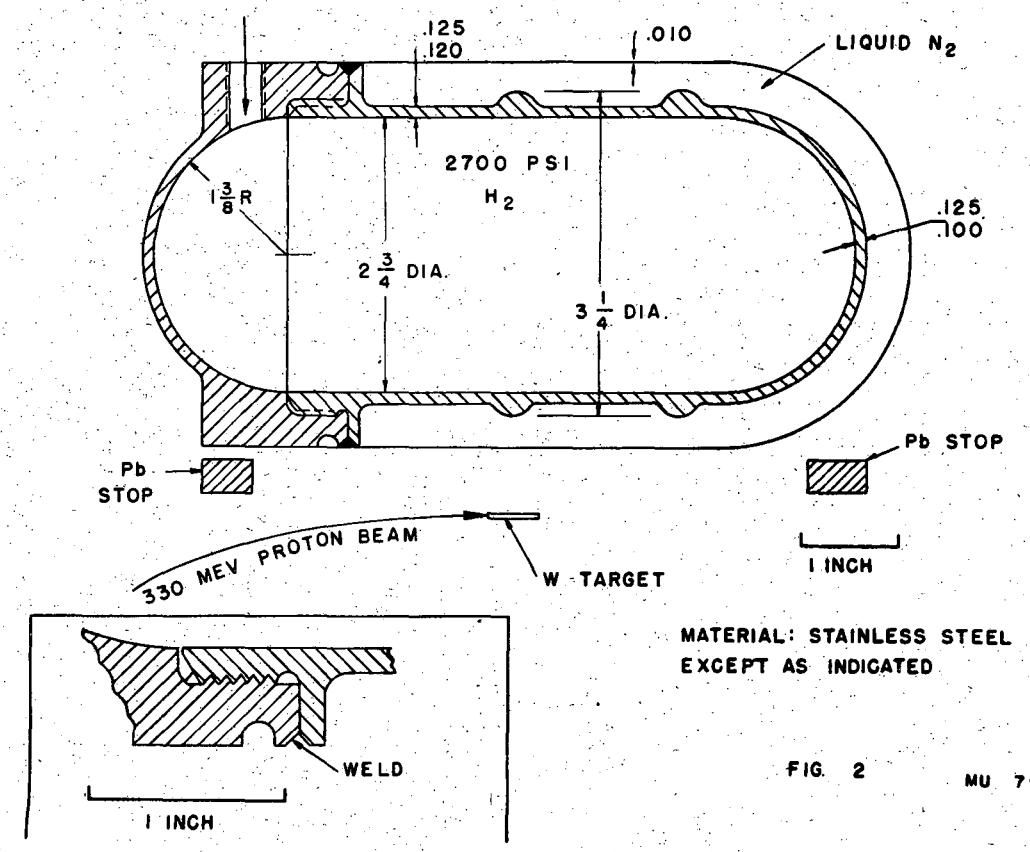

MATERIAL: STAINLESS STEEL
EXCEPT AS INDICATED

FIG. 2 MU 798

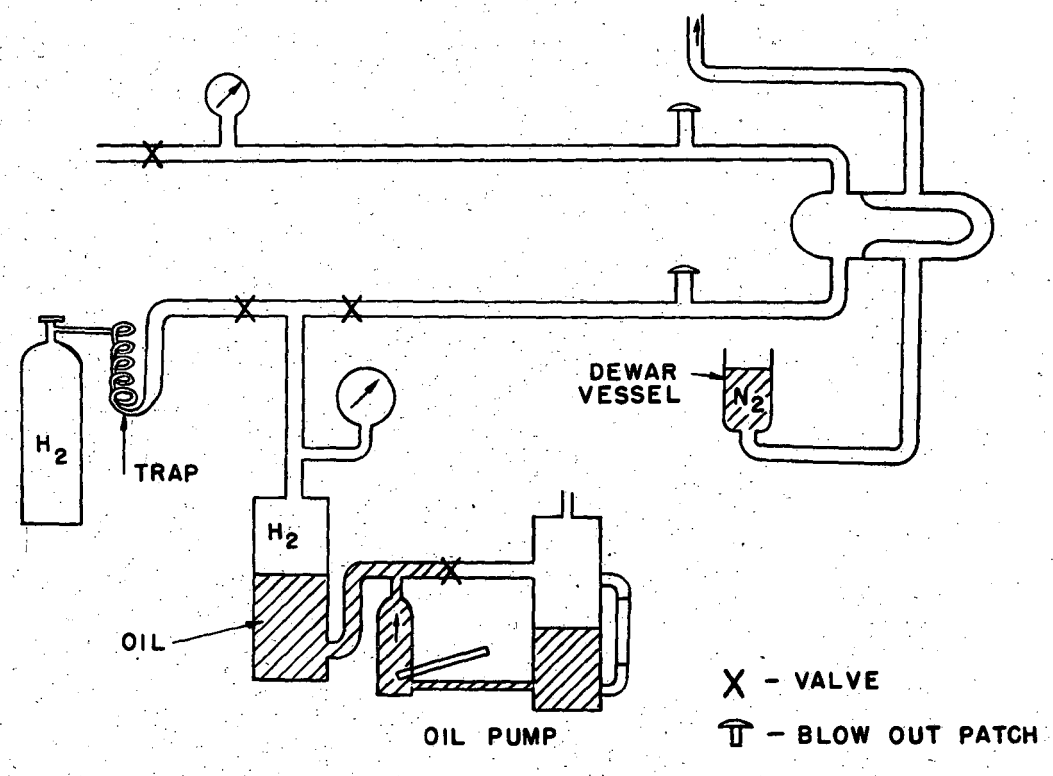

FIG. 3

MU 797

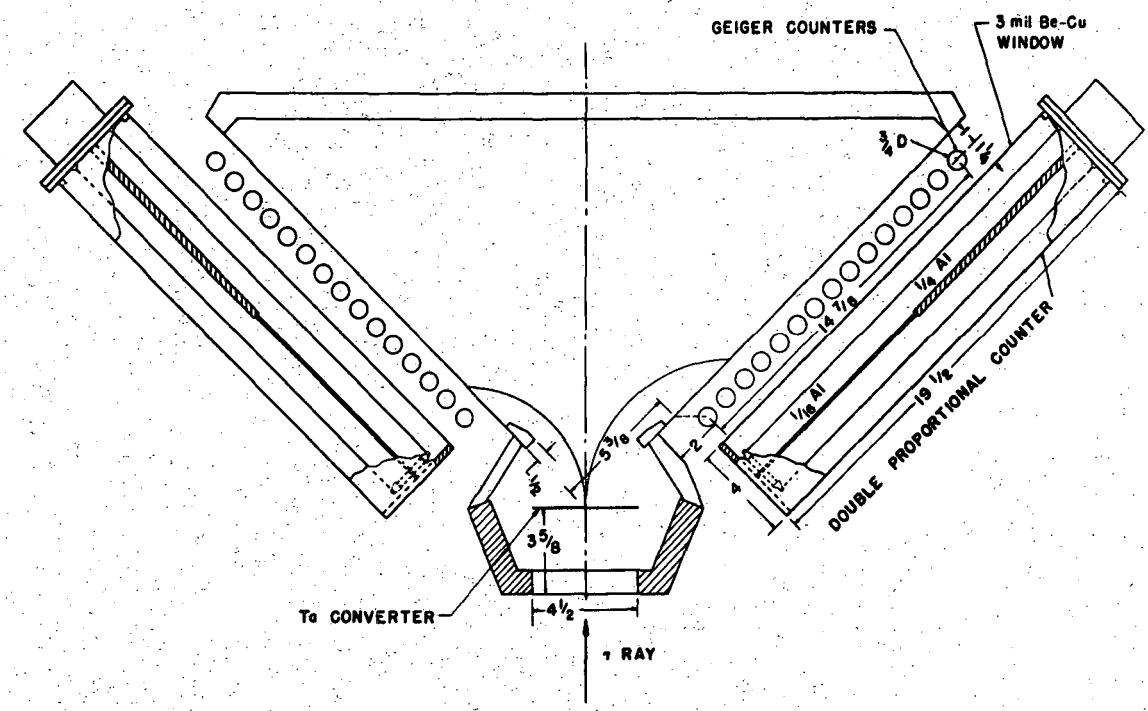
GEIGER COUNTERS
3 mil Be-Cu WINDOW
3/4 D
1 1/8
14 7/8
1/4 Al
1/16 Al
19 1/2
DOUBLE PROPORTIONAL COUNTER
5 5/8
2
4
1/8
3 5/8
4 1/2
Ta CONVERTER
γ RAY

FIG. 4

MU 794

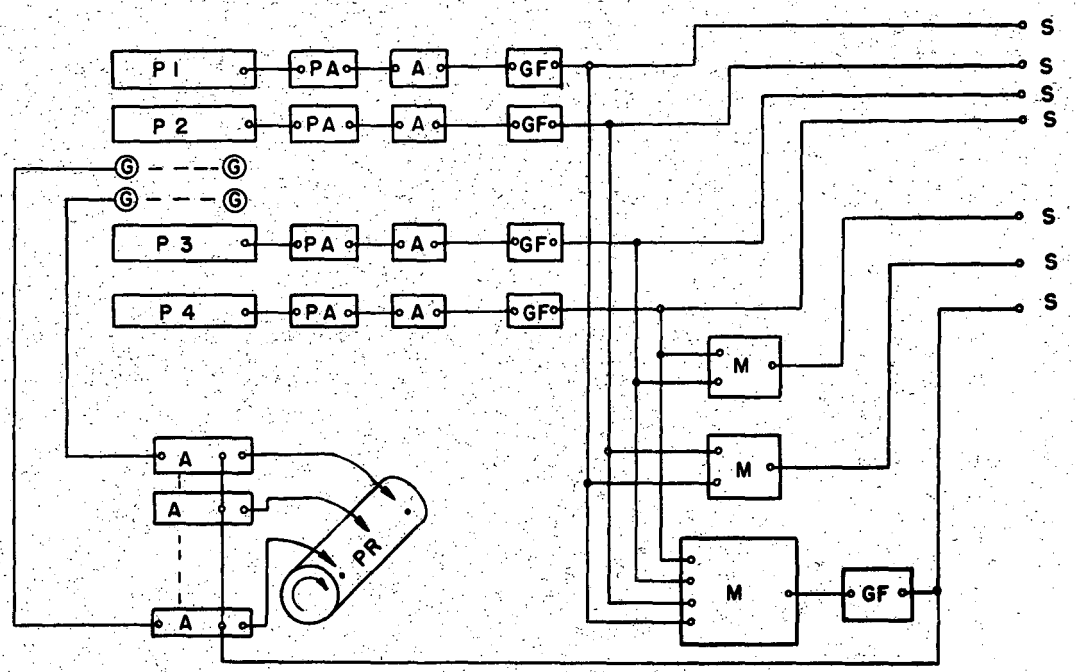

P - PROPORTIONAL COUNTER
G - GEIGER COUNTER
A - AMPLIFIER
GF - GATE FORMING UNIT
S - SCALER
PA - PRE- AMPLIFIER
M - MIXER
PR - 32 PEN RECORDER

FIG. 5

MU 792

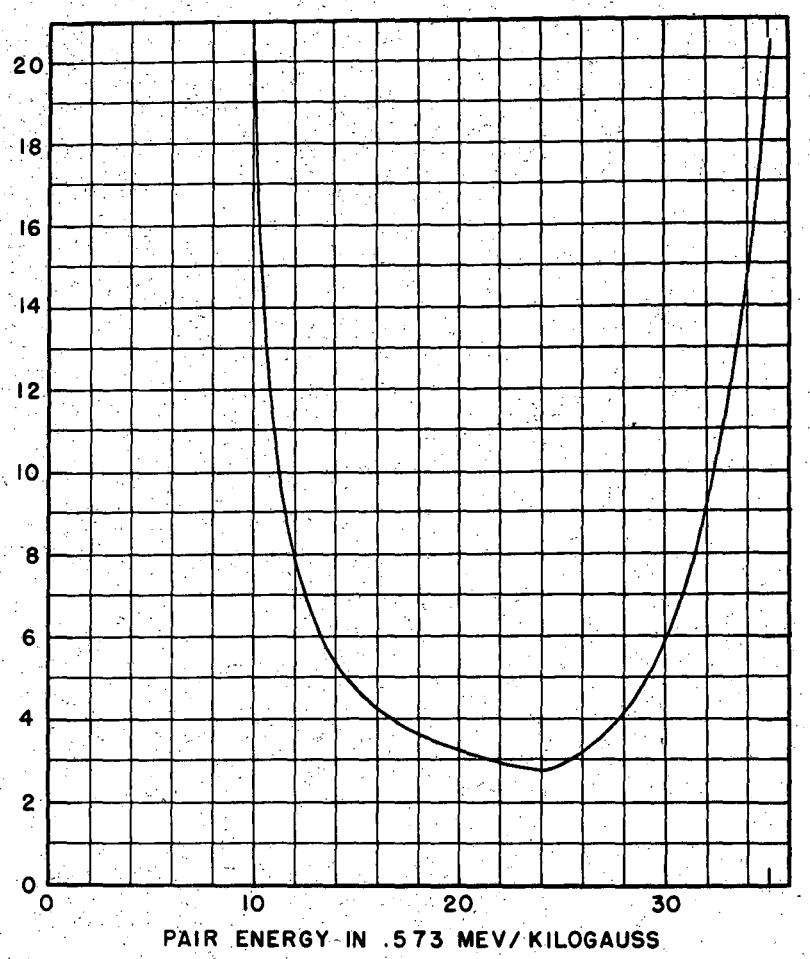
20
18
16
14
12
10
8
6
4
2
0
0
10
20
30
PAIR ENERGY IN .573 MEV/KILOGAUSS

MU 826

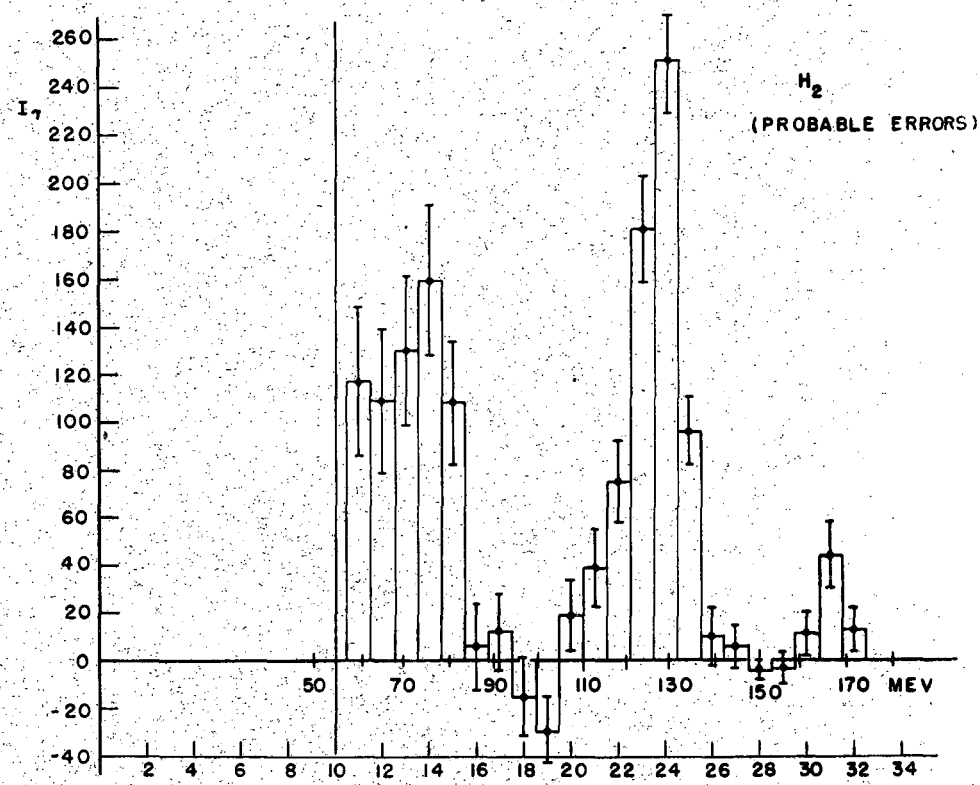
H_2
(PROBABLE ERRORS)
I_γ
260
240
220
200
180
160
140
120
100
80
60
40
20
0
-20
-40
50
70
90
110
130
150
170 MEV
2
4
6
8
10
12
14
16
18
20
22
24
26
28
30
32
34

FIG 7

MU 793

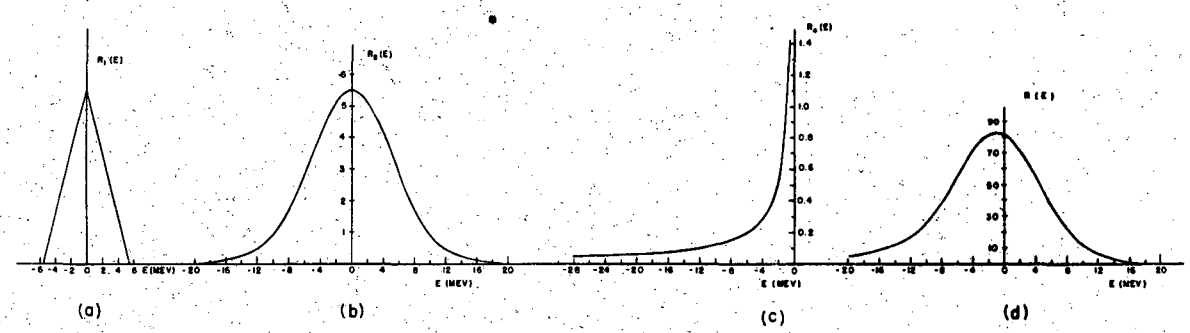

MU 823

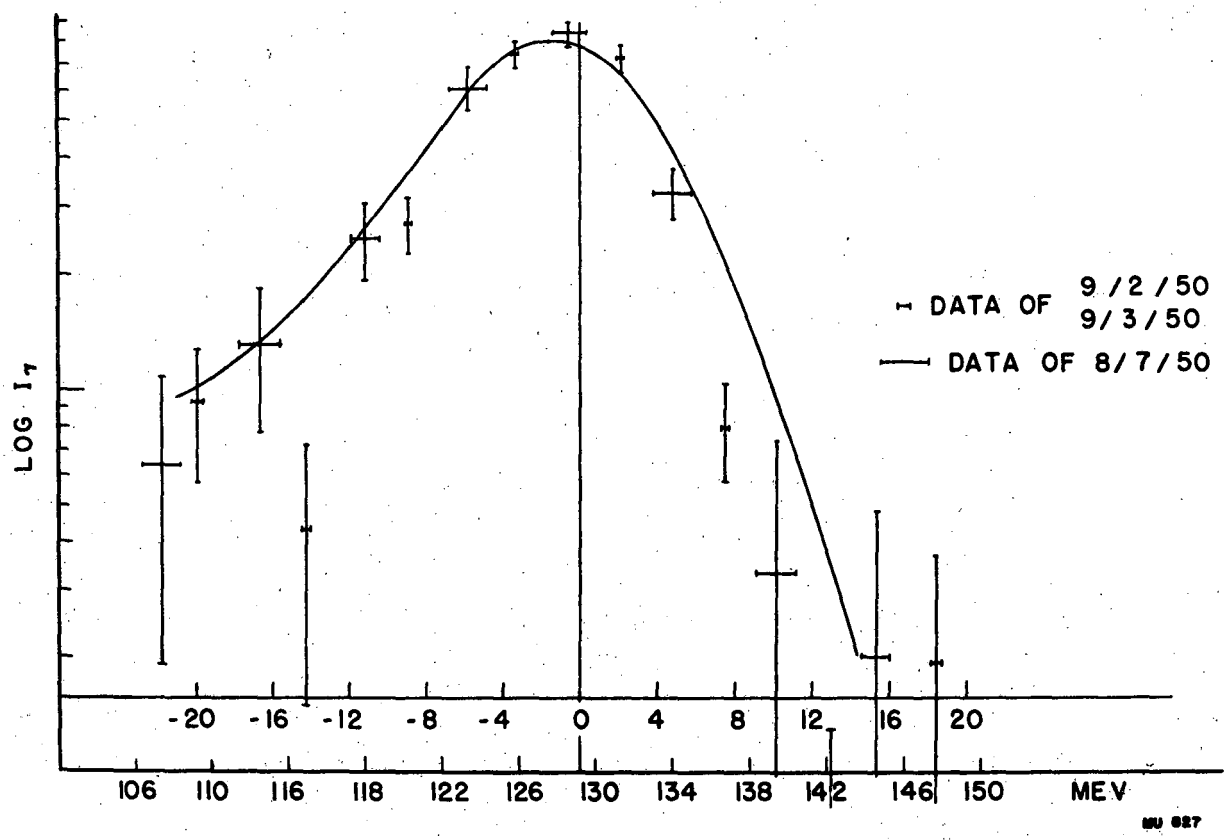
LOG I_γ
DATA OF 9/2/50 9/3/50
DATA OF 8/7/50
-20 -16 -12 -8 -4 0 4 8 12 16 20
106 110 116 118 122 126 130 134 138 142 146 150 MEV
MU 827

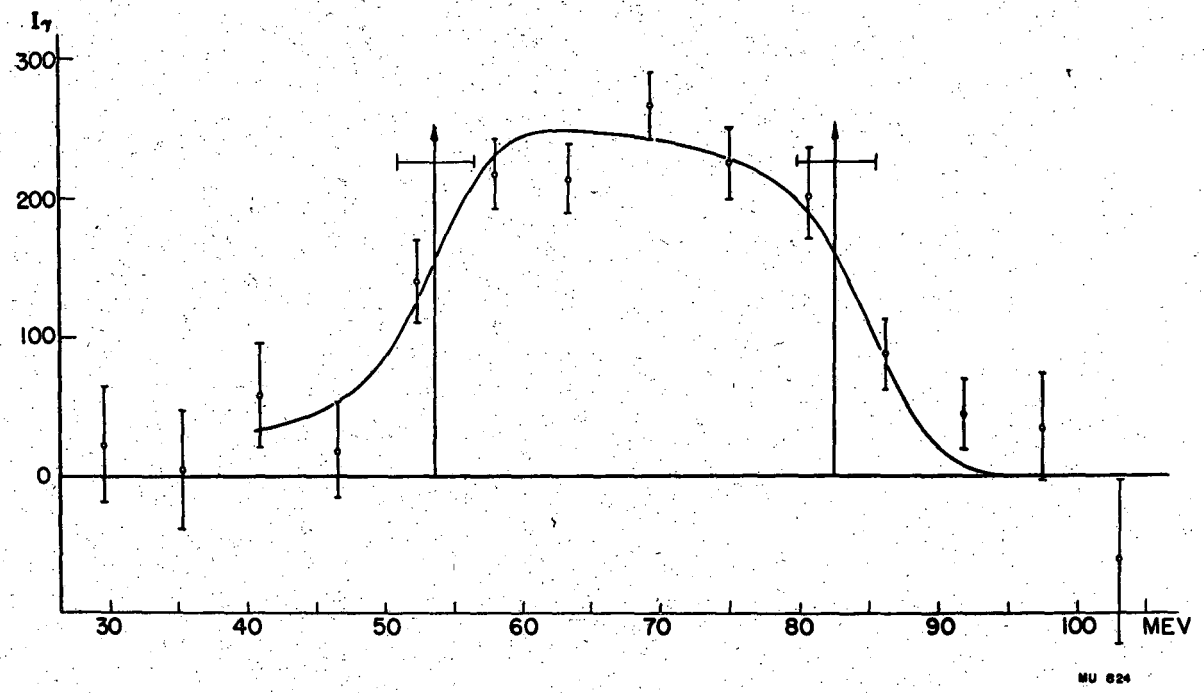
I_γ
300
200
100
0
30
40
50
60
70
80
90
100
MEV
MU 624

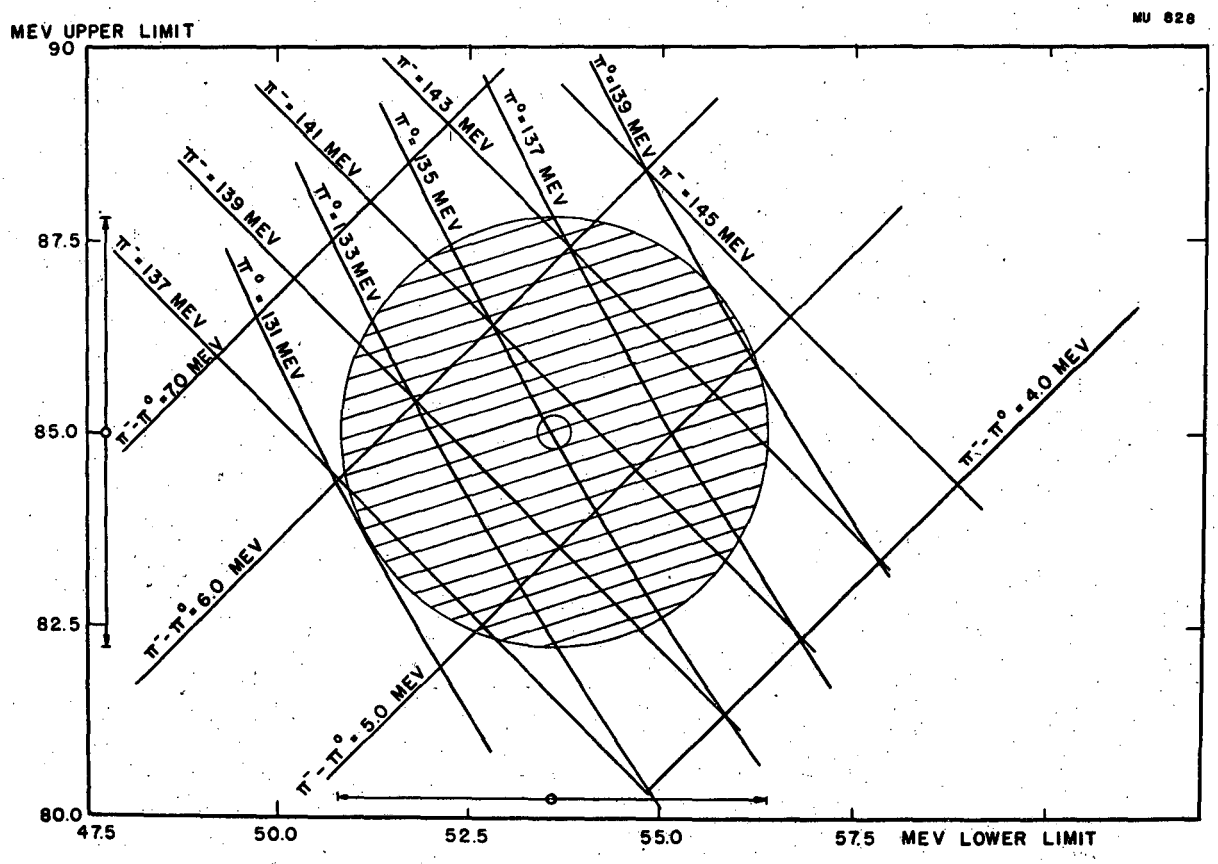
MU 828
MEV UPPER LIMIT
90
87.5
85.0
82.5
80.0
47.5
50.0
52.5
55.0
57.5
MEV LOWER LIMIT
π⁻ = 143 MEV
π⁰ = 137 MEV
π⁰ = 139 MEV
π⁻ = 141 MEV
π⁰ = 135 MEV
π⁻ = 139 MEV
π⁻ = 145 MEV
π⁰ = 133 MEV
π⁻ = 137 MEV
π⁰ = 131 MEV
π⁻ - π⁰ = 7.0 MEV
π⁻ - π⁰ = 4.0 MEV
π⁻ - π⁰ = 6.0 MEV
π⁻ - π⁰ = 5.0 MEV

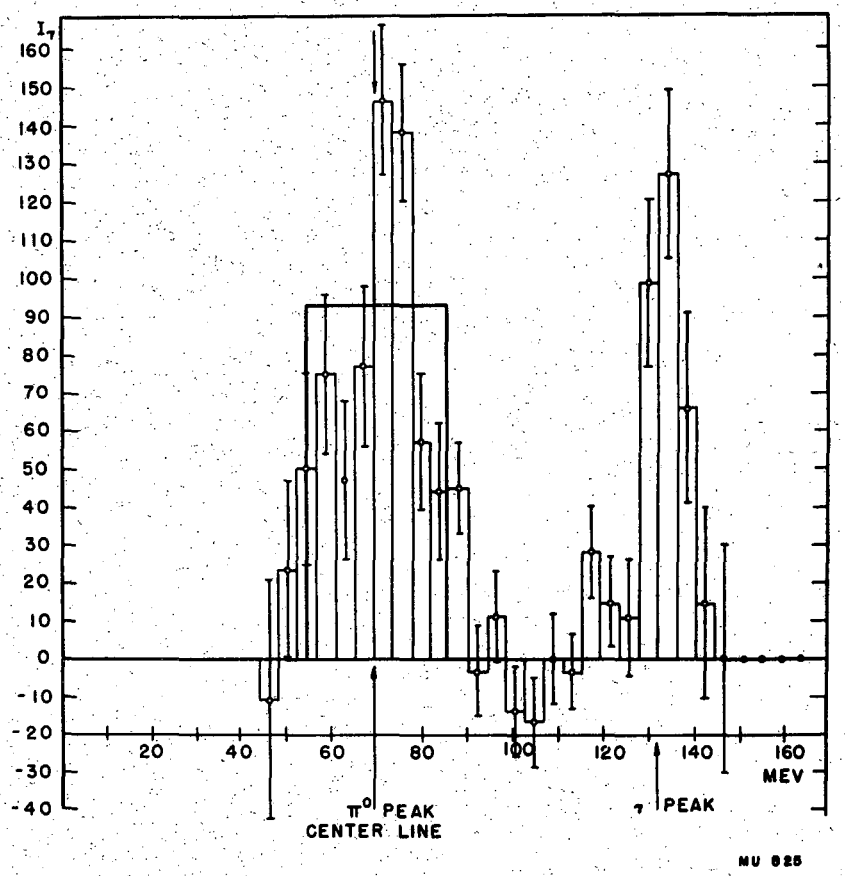
I_γ
160
150
140
130
120
110
100
90
80
70
60
50
40
30
20
10
0
-10
-20
-30
-40
20
40
60
80
100
120
140
160
MEV
π^0 PEAK
CENTER LINE
γ PEAK
MU 825

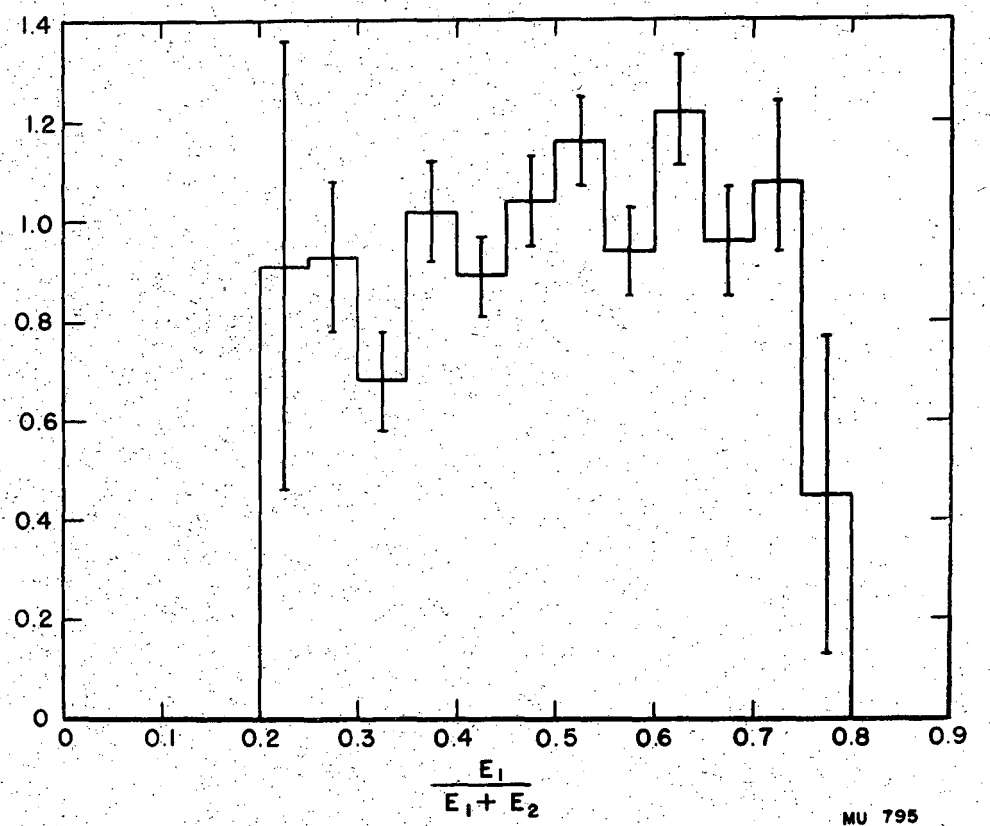

MU 795

FIG. 13

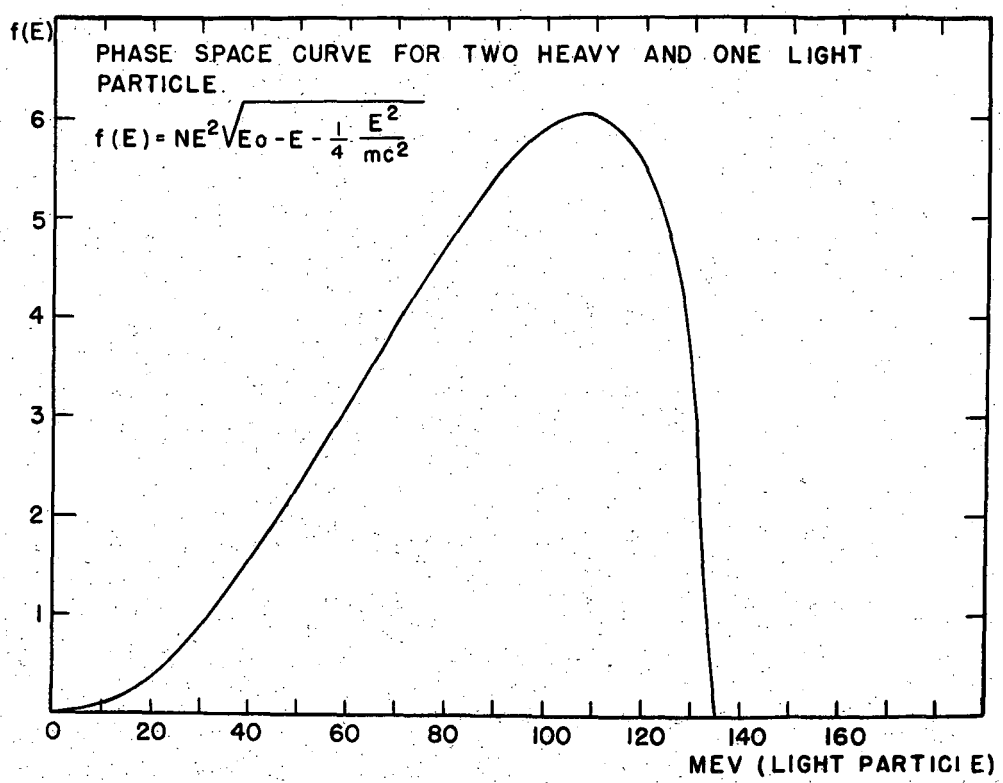
f(E)
PHASE SPACE CURVE FOR TWO HEAVY AND ONE LIGHT PARTICLE.
$f(E) = NE^2\sqrt{E_o - E - \frac{1}{4}\frac{E^2}{mc^2}}$
6
5
4
3
2
1
0
20
40
60
80
100
120
140
160
MEV (LIGHT PARTICLE)

FIG 14

MU 796

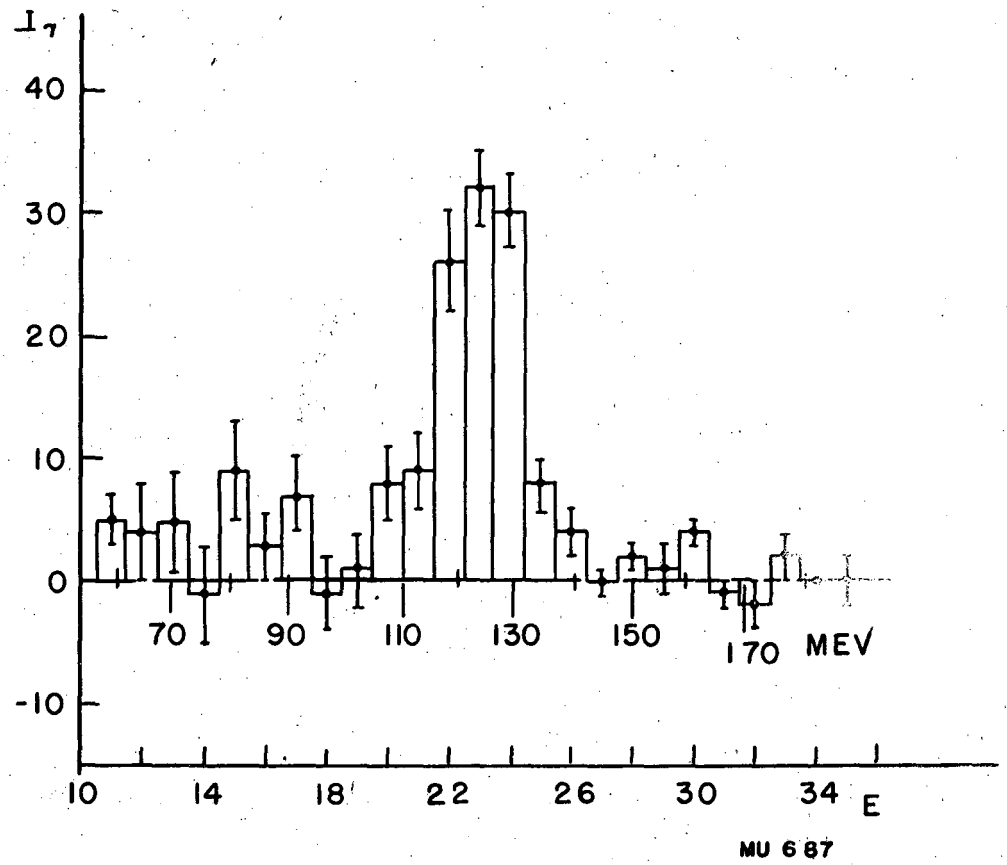
I_γ
40
30
20
10
0
-10
70
90
110
130
150
170
MEV
10
14
18
22
26
30
34
E
MU 6 87